Nanoscale

PAPER

View Article Online
View Journal | View Issue

Published on 22 May 2014. Downloaded by Iowa State University on 27/06/2017 02:24:36.

Cite this: *Nanoscale*, 2014, **6**, 8822

Corrugated epitaxial graphene/SiC interfaces: photon excitation and probing

Xiaoduan Tang, Shen Xu and Xinwei Wang*

Received 21st January 2014
Accepted 16th May 2014

DOI: 10.1039/c4nr00410h

www.rsc.org/nanoscale

Localized energy exchange and mechanical coupling across a few nm gap at a corrugated graphene–substrate interface remain great challenges to study. In this work, an infrared laser is used to excite an unconstrained epitaxial graphene/SiC interface to induce a local thermal non-equilibrium. The interface behavior is uncovered using a second laser beam for Raman excitation. Using Raman peaks for dual thermal probing, the temperature difference across a gap of just a few nm is determined precisely. The interfacial thermal conductance is found to be extremely low: 410 ± 7 W m^{-2} K^{-1}, indicating poor phonon transport across the interface. By decoupling of the graphene's mechanical and thermal behavior from the Raman wavenumber, the stress in graphene is found to be extremely low, uncovering its flexible mechanical behavior. Based on interface-enhanced Raman, it is found that the increment of interface separation between graphene and SiC can be as large as 2.9 nm when the local thermal equilibrium is destroyed.

1. Introduction

In the recent experimental study of free-standing graphene, it has been demonstrated that ripples are an intrinsic feature of graphene sheets.[1,2] Intrinsic and extrinsic corrugation of graphene flakes deposited on a SiO_2 substrate was examined using scanning tunneling microscopy (STM) and atomic force microscopy (AFM).[3,4] The nature of the height fluctuations has been addressed by Monte Carlo simulations based on the accurate description of bonding in carbon.[5] Molecular dynamics simulations were carried out to study ripple structures in graphene nanoribbons on SiC.[6] Even at equilibrium, graphene could be partly bonded with its substrate and to some extent freely suspended on its substrate. Thus the energy coupling at the interface between graphene and the substrate could be poor due to the weak bonding. To this end, very little research has been done on energy transport across graphene/substrate interfaces.[7–11] The first work by Chen *et al.* used a second metal coating (Au) on sandwiched graphene between two SiO_2 layers to facilitate the measurement with the 3ω technique.[7] Koh *et al.* and Hopkins *et al.* reported the thermal conductance at Au/Ti/graphene/SiO_2 and Al/graphene/SiO_2 interfaces.[8,9] In these ways, graphene was sandwiched between structures and the phonon mode was strongly altered. Moreover, the graphene/substrate interface can be significantly changed during this sandwiched structure preparation. The thermal conductance of the graphene/SiO_2 interface was determined varying from 2000 to 11 000 W cm^{-2} K^{-1} by Mak *et al.* in 2010.[10] The large dispersion reflected the relatively poorly defined nature of the interface between exfoliated graphene and SiO_2. Our previous work reported an anomalous interfacial thermal resistance to be 5.30×10^{-5} m^2 K W^{-1} between epitaxial graphene and SiC.[11] It was speculated that interface delamination under heating was the main reason for such poor interface energy coupling. The contact condition at the graphene and substrate interface is a main factor in determining the interfacial phonon coupling and energy exchange.

The ultra-high thermal conductivity of graphene prompts potential applications for heat removal in semiconductor devices.[12–16] It is possible for this 2-D material to effectively dissipate heat in the next generation 3-D electronics. Heat dissipation in the in-plane direction would be greatly impeded due to the thin thickness of graphene (at the atomic level).[15,17] The thermal transport to the adjacent materials plays a major role in heat dissipation instead. Therefore, knowledge of energy coupling at the interface is important to evaluate the interfacial heat dissipation and the mismatch of graphene and its substrate. Our previous work on thermal transport across the graphene/SiC interface pioneered the effort for thermal probing across the interface using Raman spectroscopy,[11] while leaving a lot of room to explore in this area. In Raman-based thermal probing, precise positioning with extremely high stability is critical for temperature measurement in order to rule out the effect of virtual dispersion due to optical misalignment at the μm scale. For interface energy flow study, non-contact localized heating is preferred over electrical heating to minimize the disturbance to the system during characterization. Although optical heating has been tried in our previous work,[11] the optical

Department of Mechanical Engineering, Iowa State University, 2010 Black Engineering Building, Ames, IA 50011, USA. E-mail: xwang3@iastate.edu; Fax: +1 515-294-3261; Tel: +1 515-294-8023

This journal is © The Royal Society of Chemistry 2014

Published on 22 May 2014. Downloaded by Iowa State University on 27/06/2017 02:24:36.

path had to be switched in order to change the laser heating power. This method introduced an undesired optical alignment effect, leading to a strong effect in the final measurement results. In Raman-based thermal probing, the wavenumber shift and Raman intensity carry very rich information (far beyond temperature) about the interface characteristics, and such study has not been explored in our last work. This work is designed and undertaken to explore all these aspects, including full non-contact photon-heating of the interface without optical alignment disturbance, interface mechanical coupling analysis based on the wavenumber, and interface spacing evaluation based on the Raman intensity enhancement. The localized selective photon-excitation makes it possible to build a well-defined energy flow across the interface. The unique photon probing based on Raman spectroscopy enables temperature difference measurement across a space of just a few nm.

2. Experimental details

2.1 Experimental setup

Epitaxial triple layer graphene (TLG) on the SiC sample ($3 \times 5 \times 1$ mm^3) is obtained from Graphene Works. Epitaxial graphene is grown on the C-face of single crystal 4H–SiC. The experimental setup for the thermal characterization of a TLG/SiC interface is shown in Fig. 1. The position of the sample is controlled by a 3-D nano-stage (MAX311D, Thorlabs). The positioning resolution of the stage, which is piezo-actuated with feedback, is down to 5 nm. The high resolution and stability of the stage are critical to the success of the measurements because they reduce the possible noise to the Raman spectra and virtual Raman shift change. Raman signals are excited by a probing laser ($\lambda = 532$ nm) and collected using a Raman spectrometer (Voyage, B&W Tek). The microscope (Olympus BX51) is confocal with the Raman spectrometer. The spot size of the Raman laser is 2×4 μm^2 (50× objective). The Raman laser power is small (6.9 mW). Although the small Raman laser spot makes the input power density high, the extremely high thermal conductivity of graphene quickly dissipates the Raman laser energy to the surrounding graphene. This lateral heat conduction becomes very important when the laser heating spot is small, and will only give a moderate temperature rise. More discussions are given in Section 2.3 for this Raman laser heating effect. Mainly, the sample is heated up by a second heating laser ($\lambda = 1550$ nm) with a continuous energy power of up to 1.6 W. The heating laser is focused by an optical lens before it irradiates the sample. The final focal spot size is 2.30×1.25 mm^2, which covers 90% of the laser energy. The heating laser irradiates from under the TLG/SiC sample with an angle of 60 to the vertical direction. The refractive indices of TLG and SiC are 2.27 and 2.56, respectively. Tri-layer graphene absorbs 6.9% of the laser energy that passes through it.[18] After multiple reflection and absorption, the TLG layer absorbs 6.98% of the incident laser energy E_0 ($0.0698E_0$). The detailed laser light trajectory and energy absorption percentage in the TLG layer is shown in Fig. 1(b).

2.2 Heat transfer model across the TLG/SiC interface

At $\lambda = 1550$ nm, the heating photon energy is less than the bandgap of SiC, so there is negligible absorption in the SiC substrate. The graphene layer is heated up and dissipates heat in three directions: one part along the graphene in-plane direction, the second part crosses the plane to the interface, and the third part dissipates to the adjacent air *via* convection and radiation. In the experiment, the temperature probing area is very small (2–4 μm) and is located in the middle of the large laser heating region (1–2 mm). So, a very little temperature gradient exists in the in-plane direction. The resulting heat transfer in the lateral direction from the thermal probing region can be neglected. For free convection of air at the sample surface, the heat transfer coefficient $h_c = (1\text{–}10)$ W m^{-2} K^{-1}. For

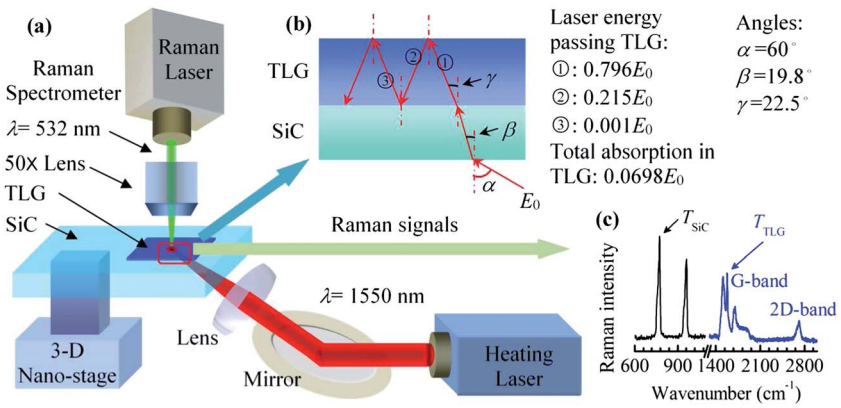

Fig. 1 Schematic of the experimental setup for characterization of the TLG/SiC interface based on photon-excitation and thermal probing. (a) A TLG/SiC sample is heated up by an infrared laser (1550 nm) from below with an incident angle of 60°. Raman signals of TLG and SiC are excited by a Raman laser (532 nm) and collected with a Raman spectrometer. The sample position is controlled by a 3-D nano-stage with a resolution of 5 nm. The graphene layer absorbs laser energy and dissipates heat to the SiC substrate across the interface. (b) The laser propagation path and the accumulated energy passing through TLG. E_0 is the energy of the heating laser reaching the TLG/SiC sample. (c) Raman spectra for both TLG and SiC layers. Their temperatures can be determined simultaneously by Raman thermometry. Also the Raman shift, linewidth, and intensity carry rich information and are used to determine the conjugated stress build-up in graphene and interface gap change.

Published on 22 May 2014. Downloaded by Iowa State University on 27/06/2017 02:24:36.

radiation, the effective heat transfer coefficient is $h_r = 4\varepsilon\sigma T^3$, where ε is the emissivity, $\sigma = 5.67 \times 10^{-8}$ W m^{-2} K^{-4}, and $T \approx$ 295 K (room temperature). Here the emissivity equals absorptivity, which is 0.069 for TLG.[18] Thus, we have $h_r = 0.4$ W m^{-2} K^{-1}. The equivalent heat transfer coefficient for combined convection and radiation is $h_c + h_r \approx 10$ W m^{-2} K^{-1} at the upper limit. The equivalent thermal resistance from the TLG surface to the adjacent air *via* convection and radiation is about 0.1 m^2 K W^{-1}. As will be detailed in the following sections, our experimental results indicate that the thermal resistance across the TLG/SiC interface is at 10^{-3} m^2 K W^{-1} magnitude. Thus, heat absorbed in graphene is mainly dissipated across the interface to the SiC substrate, and causes a temperature rise of SiC. The heat transfer to the adjacent air by convection and radiation can be neglected.

2.3 Temperature determination by the Raman spectrum

To determine the thermal conductance across the TLG/SiC interface, Raman spectra of TLG and SiC are obtained during laser heating. The graphene layer is found triple-layered according to the line shape of a 2D peak and the Raman intensity ratio of 2D peak to G peak, as shown in Fig. 1(c).[19,20] The 2D-band reveals a symmetric shape with a sharp peak, and the intensity of the G-band is less than twice the height of the 2D-band. In the layer number determination experiments, the heating laser was turned off to avoid high temperature and stress rise. The temperature rise due to the Raman laser heating is negligible. There are also monolayer and bilayer graphene on the sample. In our measurements, a TLG area was selected as it can absorb more laser energy than monolayer and bilayer graphene. Under the same power of heating laser irradiation, the temperature rise of TLG would be higher, which improves the accuracy of measurements. The Raman integration time for SiC and TLG is 4 s and 40 s, respectively. The E_2 peak ($\sim$775 cm^{-1}) of SiC is chosen for temperature determination due to its high intensity. The second order E_2 mode ($\sim$1515 cm^{-1}) of SiC is weak and partly overlaps with the G-band ($\sim$1580 cm^{-1}) of graphene. The resolution of the Raman spectrometer is 1–2 cm^{-1}. To determine precise Raman parameters, the E_2 peak of SiC is fitted with a Gaussian function. Double peak fitting with a Lorentz function is used to resolve the G peak of graphene from the second order E_2 peak of SiC. The 2D band of graphene was not used because of its broader frequency range of the peak and weak intensity. Based on the Raman spectra, the temperatures of both TLG and SiC layers are obtained under different heating laser energies.

In the measurement, the focal level of the Raman laser, which has a significant effect on Raman spectra, is first determined. When the Raman laser is focused on the graphene layer, the intensity of the G peak is strong. A group of Raman spectra are obtained at several focal levels in the vertical direction. The background signal is subtracted to achieve a sound Raman spectrum. The sample is fixed at the focal level that gives the highest graphene G peak intensity. This ensures the same focal status of the probing laser in the experiments. While heating the sample, only the power of the heating laser is increased, and no equipment is touched or changed. In this manner, the effects of environmental changes are eliminated. It ensures the maximum measurement accuracy. In the measurement, the Raman laser also heats up graphene and the substrate. The heating induced by the Raman laser does not affect the results, however. First, all the results are obtained without changing the power of the Raman laser. The temperature rise caused by the Raman laser ΔT_{Raman} is independent of that of the heating laser ΔT_{HL}. The total temperature rise is a linear addition of ΔT_{Raman} and ΔT_{HL}. ΔT_{Raman} is controlled unchanged in our whole experiment. The change in temperature rise observed *versus* the heating laser power variation is only induced by the heating laser while the effect of the Raman laser is subtracted in the linear fitting process (detailed later). Second, the power of the Raman laser (6.9 mW) is much smaller than that of the heating laser (0.1–1.6 W). The Raman spectra of the TLG/SiC sample is checked with the Raman laser power of 1 mW and 7 mW. No obvious spectral change is observed based on the graphene G peak and SiC E_2 peak. Due to the high thermal conductivity of graphene and the small size of the focal spot of the Raman laser, most of the Raman laser energy absorbed in graphene would dissipate in the in-plane direction. According to the calculations in ref. 11, the in-plane thermal resistance was determined to be 1.45×10^5 K W^{-1} if graphene has a thermal conductivity of 2000 W m K^{-1}. The overall thermal resistance at the interface within the laser-heating region can be evaluated based on the measured thermal-contact resistance. Here, our measured thermal contact resistance is 2.44×10^{-3} m^2 K W^{-1} and the spot area of the Raman laser is 8×10^{-12} m^2. The overall thermal resistance is 3.05×10^7 K W^{-1}, which is about 210 times higher than that in the in-plane direction. Therefore, only 0.47% of the absorbed laser energy would transport directly through the interface. If graphene has a higher thermal conductivity, even less energy will transfer across the graphene/SiC interface. Thus, the temperature rise induced by the Raman laser will have a negligible effect on our interface characterization.

Although a lower Raman laser energy has been used in the past for Raman spectrum study of graphene, such a low energy level is not appropriate for our interface study. In our experiment, the scattered heating laser reflected from the sample can heat the sample holder and cause the holder shift in the z direction. A screw is fixed to the holder on one end and the sample is placed on the other end. When the screw is heated by the heating laser, it moves by a very small distance ($\sim$several nanometers). On the other hand, the sample is moved by several μm or more due to the law of the lever. Such a sample position drift will induce very strong virtual scattering and Raman peak change, and needs to be addressed very carefully. We choose the laser power of 6.9 mW in order to obtain sound spectra within a very short time before the stage thermal-drift becomes important.

3. Results and discussion

3.1 Poor interface reflected by weak interfacial phonon coupling

The Raman intensity, wavenumber, and linewidth all can be employed to determine the temperature of materials. The

 This journal is © The Royal Society of Chemistry 2014

Published on 22 May 2014. Downloaded by Iowa State University on 27/06/2017 02:24:36.

Raman intensity and wavenumber decrease, and linewidth broadens with the temperature of graphene and SiC. As the linewidth is closely relevant to the phonon lifetime, it is strongly affected by the temperature of the material with little effect from stress. Therefore, the linewidth method is used to determine the temperature of both graphene and SiC, and then to evaluate the interfacial thermal conductance. Besides the temperature, the wavenumber is also dependent on the local stress in materials. Thus, the wavenumber-based temperature would be different from that based on the linewidth if a local stress exists. For Raman intensity, the light interference at the graphene/SiC interface (if local spacing exists) is a very strong influence factor in addition to temperature. Interference at the TLG/SiC interface enhances the Raman intensity.

Linewidth broadening is first employed to characterize the energy transport across the TLG/SiC interface. The temperature coefficients of TLG and SiC for the linewidth are calibrated in order to determine the local temperature during the laser heating experiment. As shown in the inset of Fig. 2(a), the temperature coefficients for TLG and SiC are 0.0187 and 0.0141 cm^{-1} K^{-1}, respectively from room temperature to 180 °C. Yue *et al.* obtained fitting slopes for TLG and SiC as 0.0127 and 0.0087 cm^{-1} K^{-1}, respectively.[11] Our calibration results agree with the literature values, considering the variation of samples and experimental environments. The thermal conductance across the TLG/SiC interface is determined to be $G_t = q''/(T_{TLG} - T_{SiC})$, where T_{TLG} and T_{SiC} are the temperatures of TLG and SiC, and q'' is the heat flux. Seven laser energy fluxes are used in the experiments to improve the accuracy of temperature determination. The temperature rise shown in Fig. 2(a) is the temperature difference of the sample heated up by the laser relative to that at room temperature. The effect of the Raman laser heating is eliminated since the Raman laser is always on regardless of the heating laser power. The temperature of the sample goes up as the laser energy flux increases. The temperature rise under no laser irradiation is adjusted to zero in order to eliminate the system error since no heat is applied at this point. The fitted slopes of temperature rise against the heat flux for TLG and SiC are 2.91×10^{-3} and 4.73×10^{-4} m^2 K W^{-1}, respectively. The interfacial thermal conductance can be determined from the slope as $G_t = 1/(T'_{TLG} - T'_{SiC})$, where T'_{TLG} and T'_{SiC} are fitting slopes of the temperature against the heat flux for TLG and SiC, respectively. The thermal conductance at the TLG/SiC interface is determined to be 410 ± 7 W m^{-2} K^{-1}. This number is extremely low and indicates rough contact and poor energy coupling at the interface. The equivalent interfacial thermal resistance for TLG/SiC is 2.44×10^{-3} m^2 K W^{-1}.

As shown in Fig. 2, the temperature rise of SiC is relatively high while our theoretical analysis gives a very low one. In our experiment, the sample is of 3×5 mm^2 in size and suspended by glass slides at two ends. The heat transfer from the SiC substrate to the glass slide is impeded, which causes the high temperature rise of SiC. At $\lambda = 532$ nm, the absorption of SiC is negligible (the corresponding optical extinction coefficient is given as "0" in references). The temperature of SiC is an average one within the focal depth of 25 μm of the Raman probing laser, or an equivalent temperature at the half focal depth. The thermal conductivity of SiC is 390 W m^{-1} K^{-1}. The heat conduction resistance within SiC is 3.21×10^{-8} m^2 K W^{-1}, which is estimated at half of the focal depth. The thermal conduction resistance in SiC is much smaller than the measured interfacial thermal resistance of 2.44×10^{-3} m^2 K W^{-1}. The effect of thermal resistance of the SiC region is negligible to the total interface thermal resistance. In the work by Yue *et al.*, the thermal contact resistance is reported as 5.30×10^{-5} m^2 K W^{-1}, which is much smaller than our measurement result.[11] The difference could be attributed to the sample to sample difference and the effect of different heating

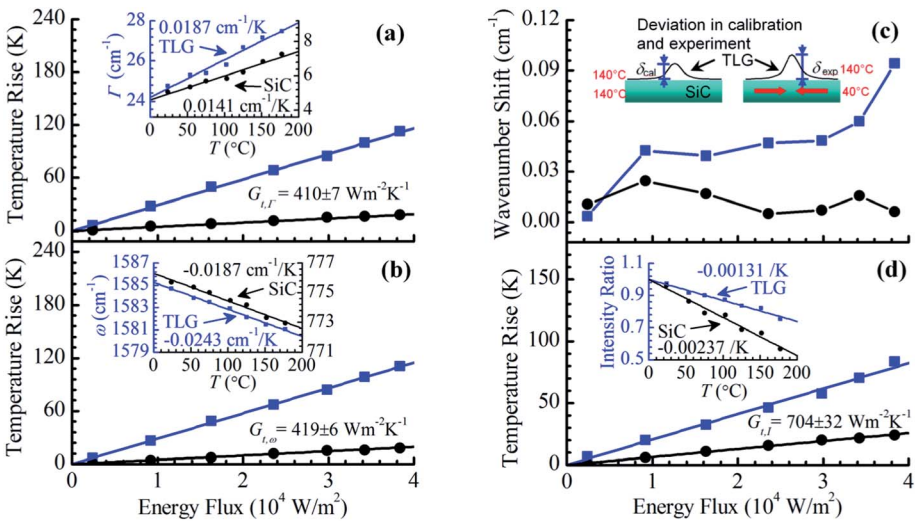

Fig. 2 Poor energy coupling at the TLG/SiC interface. (a, b and d) Interfacial thermal conductance (energy coupling rate) at the TLG/SiC interface determined by linewidth (Γ), wavenumber (ω), and intensity (I) methods. The insets show the temperature dependence on linewidth, wavenumber, and intensity for TLG and SiC, respectively. (c) Stress induced wavenumber shift for TLG and SiC. The inset shows deviation of the separation layer in the experiment and calibration due to the thermal expansion mismatch between TLG and SiC. Very little stress is built up in TLG and SiC, proving the weak mechanical coupling between them. —■—: TLG; —●—: SiC.

Published on 22 May 2014. Downloaded by Iowa State University on 27/06/2017 02:24:36.

conditions. Molecular dynamics simulations in ref. 11 reported a TLG/SiC thermal resistance of 7.01×10^{-10} m^2 K W^{-1} for an interface covalent bond. Our experimental value is 7 orders of magnitude higher than the simulation result. The extremely large thermal contact resistance indicates a very weak contact at the TLG/SiC interface. A detailed discussion is provided in the following to interpret the result.

3.2 Poor interface coupling revealed by negligible stress in graphene upon laser heating

A. Thermal conductance analysis based on the Raman wavenumber. The above measured very small interface thermal conductance indicates that the TLG has a loose contact with the SiC substrate. This loose contact will have very limited constraint on graphene movement. This means under local heating, the thermal expansion mismatch at the interface will induce little stress in graphene. In other words, under local heating, the stress build-up in graphene can be used as an indicator to explore the local mechanical coupling strength. Weak mechanical coupling will lead to little stress in graphene, and help explain the extremely weak interface energy coupling observed above.

To explore the TLG–SiC interface mechanical coupling, the Raman wavenumber is evaluated at various heating levels. The wavenumber is related to both temperature and stress, and it is more sensitive to temperature than the linewidth. Thus the local stress can be reflected by the temperature difference between wavenumber and linewidth methods. Thermal expansion of TLG and SiC should be considered in explaining the thermal stress due to the significant difference between their thermal expansion coefficients. During laser heating, a large local stress would arise due to the mismatch of the thermal expansions if perfect bonding exists between TLG and SiC. Otherwise, a rough contact at the interface would lead to a small stress. First of all, we evaluate the temperature rise in TLG and SiC based on the wavenumber while the stress effect is not subtracted, and then use this temperature rise to calculate the interface thermal conductance. We intend to prove that even under the effect of stress, the wavenumber method gives an interface thermal conductance very close to that determined based on Raman linewidth analysis. This provides solid evidence that the stress in graphene and Si indeed is very small during the experiment and the mechanical coupling at the interface is weak. Then we perform quantitative analysis of the stress build-up in SLG and graphene.

The temperature coefficients of the wavenumber for TLG and SiC are calibrated and shown in the inset of Fig. 2(b). The wavenumber decreases with slopes of -0.0243 and -0.0187 cm^{-1} K^{-1} for the G-band of TLG and E_2 mode of SiC, respectively. Yue *et al.* obtained temperature coefficients of -0.025 and -0.016 cm^{-1} K^{-1} for TLG and SiC, respectively.[11] The slope of the temperature against the wavenumber was reported in a range from -0.015 to -0.038 cm^{-1} K^{-1} for single and bilayer graphene.[21–23] The temperature coefficient for graphene varies with the number of layers, the wavelength of probing lasers, and the calibrated temperature range. Harima *et al.* reported a temperature coefficient of 6H–SiC as -0.023 cm^{-1} K^{-1} in a temperature range from 0 to 1000 °C.[24] Thus, our calibration results are in good agreement with the literature values. The fitting slopes of the temperature rise against the heat flux for TLG and SiC are 2.87×10^{-3} and 4.85×10^{-4} m^2 K W^{-1}, respectively. The thermal conductance at the TLG/SiC interface is determined to be 419 ± 6 W m^{-2} K^{-1} based on the wavenumber method. This result is nearly the same with the one obtained by the linewidth. This strongly proves that the temperature rise on the basis of the linewidth was affected very little by the stress, or the stress change in the corrugated graphene is very small. This confirmed that there was little stress change in the sample during laser heating, and its effect on the linewidth is negligible. It needs to be pointed out that the calibration results shown in Fig. 2(b) and the temperature determined using the wavenumber in Fig. 2(b) all have the effect of stress build-up during the calibration and laser-heating experiment, even when this stress is small. The level of this stress could be a good indicator of the flexibility of graphene on SiC. Below we detail how to evaluate the stress build-up in graphene based on the Raman wavenumber.

B. Stress-level analysis for TLG and SiC. In the laser heating experiment, at one specific laser heating level E, we could obtain the temperature of graphene, T_{TLG}, based on the Raman linewidth, which has little effect on stress. Using this temperature and the Raman wavenumber-T calibration result shown in Fig. 2(b) (inset), an expected wavenumber shift for graphene can be calculated ($\Delta\omega_{\mathrm{cal}}$). Note that in calibration, TLG and SiC have the same temperature, so $\Delta\omega_{\mathrm{cal}}$ is the wavenumber shift of graphene at temperature T_{TLG} when the SiC substrate is also at the same temperature. The interfacial thermal expansion mismatch between TLG and SiC gives rise to a stress in graphene during calibration. Therefore, $\Delta\omega_{\mathrm{cal}}$ consists of two parts: one by temperature rise, $\Delta\omega_{\mathrm{cal},T}$, and the other one by stress in graphene during calibration, $\Delta\omega_{\mathrm{cal},\sigma}$. In our interface thermal conductance measurement experiment, the temperature of TLG is always higher than that of the SiC substrate as shown in Fig. 2(a), and the graphene's wavenumber shift is directly measured as $\Delta\omega_{\mathrm{exp}}$. Similarly, we also have $\Delta\omega_{\mathrm{exp}} = \Delta\omega_{\mathrm{exp},T} + \Delta\omega_{\mathrm{exp},\sigma}$. Here $\Delta\omega_{\mathrm{exp},T}$ should be equal to $\Delta\omega_{\mathrm{cal},T}$, but $\Delta\omega_{\mathrm{exp},\sigma}$ is the wavenumber shift induced by stress in graphene, and should be different from $\Delta\omega_{\mathrm{cal},\sigma}$.

The above scenario can be better explained by the inset in Fig. 2(c), which shows the morphology change of graphene from calibration to the laser heating experiment. Based on the temperature rise shown in Fig. 2(a), we know that when the temperature of TLG reaches 140 °C, the SiC surface will have a temperature of 40 °C. But in calibration, when TLG is at 140 °C, the SiC surface is at the same temperature. So comparing the scenarios of calibration and the laser heating experiment shown in Fig. 2(c), even graphene has the same temperature, and the SiC substrate has a contraction from calibration to laser heating experiment. This contraction will induce a stress change in graphene from calibration to laser heating experiment. This SiC contraction-induced wavenumber change in graphene can be calculated as $\Delta\omega_{\mathrm{exp}} - \Delta\omega_{\mathrm{cal}}$. The result is shown in Fig. 2(c). Similarly we calculate the Raman wavenumber change by stress level change in SiC, and also the results are shown in Fig. 2(c).

 This journal is © The Royal Society of Chemistry 2014

Published on 22 May 2014. Downloaded by Iowa State University on 27/06/2017 02:24:36.

The stress induced wavenumber shift [Fig. 2(c)] for TLG is less than 0.1 cm^{-1}, and for SiC, it is even smaller. Therefore, it is conclusive that graphene experiences very little stress during laser heating, and poor contact at the TLG/SiC interface is responsible for such flexible movement of TLG. Graphene can change the profile on the SiC surface with a large degree of freedom during laser heating. The separation of TLG and SiC causes large thermal contact resistance at the interface. For SiC, we observed negligible stress change in it between the calibration and laser heating experiment. This again proves that TLG and SiC have a loose contact, and no tight mechanical coupling exists between them.

3.3 Graphene/SiC separation revealed by AFM surface morphology and enhanced Raman

A. AFM surface morphology study. To confirm the poor contact at the TLG/SiC interface and obtain a quantitative idea about the interface corrugation, AFM imaging is carried out on the TLG/SiC sample and also on bare SiC for comparison. AFM images of several spots on the sample were taken to check the occurrence of corrugations. Typical surface height variations of the TLG/SiC and bare SiC samples are shown in Fig. 3(a–d). Many ripples of TLG can be found in the AFM image. Only a small portion of TLG is in contact with the SiC substrate. The height of the red line in the TLG image varies from 0.8 to 6.3 nm, with an average height of 2.1 nm. The height variation of bare SiC is mainly concentrated in a range from 0.7–1.3 nm, with an average height of 0.3 nm. The AFM results indicate a high average separation distance between TLG and SiC.

B. Interfacial thermal conductance based on the Raman intensity. The separation between TLG and SiC will give rise to interference for the Raman signals. Raman intensities of TLG and SiC are analyzed to explain the roughness of the sample. In addition, it can be employed to evaluate the separation distance increment between TLG and SiC upon laser heating.[25,26] The Raman intensity decreases with the temperature of the material. Usage of the absolute intensity difference is hard to

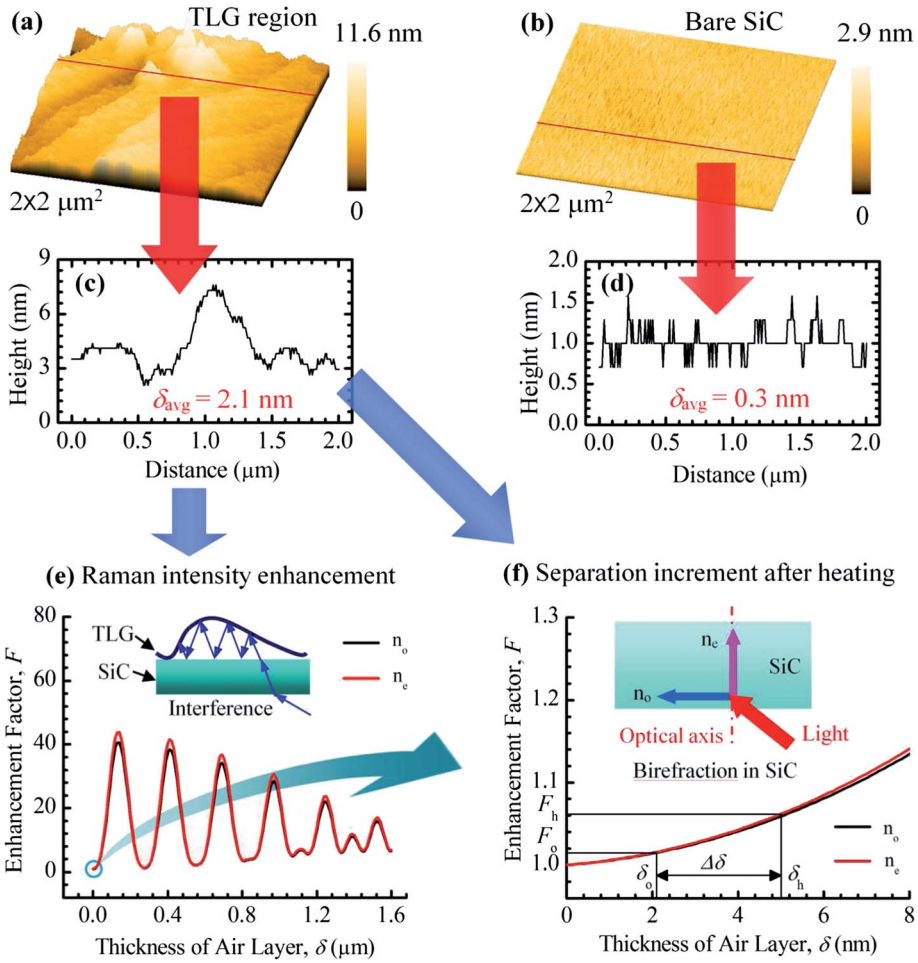

Fig. 3 Nanoscale weak contact at the TLG/SiC interface. (a and b) AFM images of TLG/SiC and bare SiC. (c and d) The height variations of the red lines shown in figures (a and b). The average heights are 2.1 and 0.3 nm for TLG/SiC and bare SiC, respectively. (e) The increment of the Raman intensity enhancement factor (F) and the thickness of the air layer (δ) between TLG and SiC. The inset shows a simplified interference model of the TLG/SiC interface. (f) The variation of F against δ while δ is less than 8 nm. δ increases from 2.1 to 5.0 nm after the laser heating experiment. The birefraction in SiC is delineated in the inset. When an unpolarized light enters SiC, the light splits into two linearly polarized beams. One beam is parallel to the optical axis (n_e), and the other is perpendicular to the optical axis (n_O).

Published on 22 May 2014. Downloaded by Iowa State University on 27/06/2017 02:24:36.

determine the temperature rise, as the intensity is sensitive to the focal level of the Raman excitation laser, configuration of the Raman system, and other experimental factors. To improve the measurement accuracy, the normalized intensity is used to determine the temperature rise. In the calibration, Raman intensities are obtained at temperatures from 25 to 180 °C. Extrapolation is carried out to get the intensities for TLG and SiC at 0 °C. The normalized intensity, which is the ratio of the intensity at a certain temperature to that at 0 °C, decreases as the temperature increases. The inset in Fig. 2(d) shows fitting slopes for the G-band of TLG and E_2 mode of SiC as −0.00131 and −0.00237 K^{-1}, respectively. To the best of our knowledge, no literature has been found about the temperature coefficients for the normalized intensity of graphene and SiC. The slopes for the temperature rise of TLG and SiC against the heat flux are 2.06×10^{-3} m^2 K W^{-1} and 6.43×10^{-4} m^2 K W^{-1}, respectively. The interfacial thermal conductance based on the Raman intensity is determined to be 704 ± 32 W m^{-2} K^{-1}. As there is a separation between TLG and SiC layers, part of the SiC Raman signals is multi-reflected by the TLG layer. The collected SiC Raman intensity increases. Consequently, the SiC temperature rise determined by Raman intensity reduction would decrease. The intensity-based thermal conductance is higher than the results based on linewidth and wavenumber methods. Three factors are considered leading to the difference: various thermal expansion conditions in the experiment and calibration, the air layer between TLG and SiC, and light interference at the interface. These factors are analyzed as below.

C. Interference-induced Raman enhancement. The thermal expansion of TLG and SiC should be considered first due to the difference in their thermal properties. The thermal expansion coefficient of graphene was reported in a range from negative values to 1×10^{-5} K^{-1},[27] while the coefficient of SiC is about 4.5×10^{-6} K^{-1}.[28] The difference causes mismatch during laser heating. In addition, the thermal expansion conditions for the experiment and calibration are different. The mismatch distance between the TLG and SiC is increased during the laser heating experiment. Take a case of graphene at 140 °C for instance. In calibration, the TLG and SiC temperatures are the same and uniformly distributed within the Raman probing area (~8 μm^2). The distance between TLG and SiC is δ_{cal}, and the probed intensity is I_{cal}. In the laser heating experiment, the temperature distribution is different. The TLG reaches 140 °C while SiC is around 40 °C according to the linewidth method. So SiC shrinks relative to the scenario with a temperature of 140 °C in calibration. Consequently, the ripple height of TLG on SiC is enlarged, which means $\delta_{exp} > \delta_{cal}$, and $I_{exp} > I_{cal}$.

Fig. 3(e) shows that the interference effect of the Raman scattering signals at the interface enhances the Raman intensity. When an unpolarized light enters SiC at a nonzero acute angle to the optical axis, the light will split into two linearly polarized beams [Fig. 3(f), inset]. The beam parallel to the optical axis has a refractive index of n_e. The other beam perpendicular to the optical axis has a refractive index of n_0. For the parallel beam (n_e), the refractive indices of SiC are 2.74 + 0i and 2.72 + 0i for incident laser and Raman scattering, respectively. For the perpendicular beam (n_0), the refractive indices of SiC are 2.68 + 0i and 2.66 + 0i for incident laser and Raman scattering, respectively. Both incident and Raman scattering lights are reflected multiple times on the air/TLG/air/SiC interfaces [Fig. 3(e), inset]. Considering the absorption and scattering of each layer, the normalized enhancement factor is calculated with optical constants of all layers.[25,26] The net absorption term (F_{ab}) is expressed as

$$F_{ab} = t_1 \frac{(1 + r_2 r_3 e^{-2i\beta_2}) e^{-i\beta_x} + (r_2 + r_3 e^{-2i\beta_2}) e^{-i(2\beta_1 - \beta_x)}}{1 + r_2 r_3 e^{-2i\beta_2} + (r_2 + r_3 e^{-2i\beta_2}) r_1 e^{-2i\beta_1}} \quad (1)$$

where $t_1 = 2n_0/(n_0 + \tilde{n}_1)$, $r_1 = (n_0 - \tilde{n}_1)/(n_0 + \tilde{n}_1)$, $r_2 = (\tilde{n}_1 - \tilde{n}_2)/(\tilde{n}_1 + \tilde{n}_2)$, and $r_3 = (\tilde{n}_2 - \tilde{n}_3)/(\tilde{n}_2 + \tilde{n}_3)$ are the Fresnel transmittance and reflection coefficients for the interfaces involving air (0), TLG (1), air (2), and SiC (3). n_0, $\tilde{n}_1$, $\tilde{n}_2$, and $\tilde{n}_3$ are the refractive indices for air, TLG, air, and SiC, respectively. $\beta_x = 2\pi x \tilde{n}_1/\lambda$, $\beta_1 = 2\pi d_1 \tilde{n}_1/\lambda$, and $\beta_2 = 2\pi d_2 \tilde{n}_2/\lambda$, x is the depth of the point where the interaction occurs, λ is the wavelength of incident laser, and d_1 and d_2 are the thickness of the graphene layer and the in-between air layer, respectively. The net scattering term (F_{sc}) is described as

$$F_{sc} = t_1' \frac{(1 + r_2 r_3 e^{-2i\beta_2}) e^{-i\beta_x} + (r_2 + r_3 e^{-2i\beta_2}) e^{-i(2\beta_1 - \beta_x)}}{1 + r_2 r_3 e^{-2i\beta_2} + (r_2 + r_3 e^{-2i\beta_2}) r_1 e^{-2i\beta_1}}, \quad (2)$$

where $t_1' = 2\tilde{n}_1/(\tilde{n}_1 + n_0)$ and λ is the wavelength of the G band of graphene. Thus, the total enhancement factor (F) is given by

$$F = N \int_0^{d_1} |F_{ab} F_{sc}|^2 dx \quad (3)$$

where N is a normalized factor, which is a reciprocal number of the total enhancement factor for the TLG layer on the SiC substrate without the air layer between them, obtained by setting the thickness of the in-between air layer to be 0. The normalized enhancement factor (F) can be as high as 1.15 as the thickness (δ) of the air layer between TLG and SiC is 8 nm, as shown in Fig. 3(f).

According to the Raman intensity enhancement in the experiment, the thickness increment of the air layer at the TLG/SiC interface between laser heating experiment and calibration can be evaluated. For instance, if under a laser heating energy flux E, the graphene has a temperature rise of ΔT. If the substrate has the same temperature as graphene just like in calibration, we expect that the normalized Raman intensity (I_{cal}/I_0) from graphene will be $1 + \Delta T\, \chi_I$, where χ_I is the temperature coefficient of the normalized intensity as shown in the inset of Fig. 2(d). Here I_0 is the Raman intensity at room temperature, and I_{exp} is the expected Raman intensity. However, in our thermal conductance measurement experiment, the normalized Raman intensity of graphene with temperature rise ΔT is measured as I_{exp}/I_0. The enhancement of normalized Raman intensity can be calculated as $\Gamma_{nor} = (I_{exp}/I_0)/(I_{cal}/I_0) = (I_{exp}/I_0)/(1 + \Delta T \chi_I)$. Due to the separation (δ) change as shown in Fig. 2(c) inset, we expect that Γ_{nor} will be greater than 1.

Based on Fig. 2(a and d), when the absorbed energy flux in TLG is 3.8×10^4 W m^{-2}, we have $\Delta T = 113.1$ K, and $\chi_I = -0.00131$ K^{-1}. Our measured normalized Raman intensity at $\Delta T = 113.1$ K is $I_{exp}/I_0 = 0.890$. The expected normalized Raman intensity without interface separation change is $(1 + \Delta T \chi_I) =$

 This journal is © The Royal Society of Chemistry 2014

Published on 22 May 2014. Downloaded by Iowa State University on 27/06/2017 02:24:36.

0.852. Therefore, we have $F_{nor} = 1.045$. Based on the AFM results, the original separation between TLG and SiC is roughly $\delta_{cal} = 2.1$ nm. So the original enhancement would be $F_o = 1.015$ as shown in Fig. 3(f). After extra intensity enhancement by $\delta_{exp} \rightarrow \delta_{cal}$, the final enhancement factor is $F_h = F_o F_{nor} = 1.061$. F_o and F_h are shown in Fig. 3(f). So based on the enhancement calculation shown in Fig. 3(f), the final separation distance will be $\delta_{exp} = 5.0$ nm for both parallel- and perpendicular-beam cases. The separation increment of the air layer is then obtained as $\Delta\delta = \delta_{exp} - \delta_{cal} = 2.9$ nm.

In the above discussion, the laser energy absorption in TLG [Fig. 1(b)] does not consider the interference effect since we do not know yet about the TLG–SiC spacing then. Following the interference study above, we know that the overall enhancement factor is 1.061. The absorption enhancement factor is less than this value, only 1.04 from our calculation. Based on this absorption enhancement factor, we can do a little adjustment to the calculated thermal conductance. The linewidth-based thermal conductance is adjusted from 419 to 436 W m^{-2} K^{-1}, and the wavenumber-based one is adjusted from 410 to 426 W m^{-2} K^{-1}. Note that this adjustment is only for the case of graphene temperature at 140 °C. For lower temperatures, the adjustment factor will be much less, and eventually negligible.

From the above discussion, we can conclude that a separation layer exists at the TLG/SiC interface, causing poor contact between epitaxial graphene and SiC substrate. The rough contact can be explained by the synthesis method of the TLG/SiC sample. Epitaxial graphene is grown on the C-face of 4H–SiC by heating the sample up to 1300 °C in a vacuum oven. During synthesis, graphene and SiC is a perfect match. When the sample is taken out of the oven, it cools down to room temperature. Graphene and SiC has different thermal expansion coefficients, so they will have different contraction, leading to interface delamination. Therefore, the interfacial thermal conductance can be very low.

4. Conclusion

The energy coupling at the epitaxial graphene/SiC interface was characterized with localized photon excitation and thermal probing. The thermal conductance between graphene and SiC was determined as low as 410 ± 7 W m^{-2} K^{-1} by Raman linewidth broadening. Such measurement was facilitated by the Raman-based dual thermal probing with a superior spatial resolution. The extremely low thermal conductance is due to corrugation at the interface, which is further confirmed by three aspects. First, the thermal conductance based on the wavenumber shift is calculated and agreed very well with that based on the linewidth method. Very little stress was built up in graphene. The graphene layer was loose on the substrate. Second, AFM imaging revealed an average distance of 2.1 nm between graphene and SiC. The graphene flake is partly supported by the SiC substrate. Finally, Raman intensity analysis yielded a much higher thermal conductance than the linewidth and wavenumber. Light interference study further proved the existence of the air layer between graphene and SiC. Strategies were developed to calculate the thickness increment of the air layer between graphene and SiC after laser heating.

Acknowledgements

Support of this work by the National Science Foundation (CMMI-1200397 and CBET-1235852) is gratefully acknowledged. X.W. thanks the great support of the "Taishan Scholar" program of Shandong Province, China.

References

1 J. C. Meyer, A. K. Geim, M. I. Katsnelson, K. S. Novoselov, T. J. Booth and S. Roth, *Nature*, 2007, **446**, 60–63.
2 C. C. Chen, W. Z. Bao, J. Theiss, C. Dames, C. N. Lau and S. B. Cronin, *Nano Lett.*, 2009, **9**, 4172–4176.
3 V. Geringer, M. Liebmann, T. Echtermeyer, S. Runte, M. Schmidt, R. Ruckamp, M. C. Lemme and M. Morgenstern, *Phys. Rev. Lett.*, 2009, **102**, 076102.
4 E. Stolyarova, K. T. Rim, S. M. Ryu, J. Maultzsch, P. Kim, L. E. Brus, T. F. Heinz, M. S. Hybertsen and G. W. Flynn, *Proc. Natl. Acad. Sci. U. S. A.*, 2007, **104**, 9209–9212.
5 A. Fasolino, J. H. Los and M. I. Katsnelson, *Nat. Mater.*, 2007, **6**, 858–861.
6 C. Tang, L. J. Meng, L. Z. Sun, K. W. Zhang and J. X. Zhong, *J. Appl. Phys.*, 2008, **104**, 113536.
7 Z. Chen, W. Jang, W. Bao, C. N. Lau and C. Dames, *Appl. Phys. Lett.*, 2009, **95**, 161910.
8 P. E. Hopkins, M. Baraket, E. V. Barnat, T. E. Beechem, S. P. Kearney, J. C. Duda, J. T. Robinson and S. G. Walton, *Nano Lett.*, 2012, **12**, 590–595.
9 Y. K. Koh, M. H. Bae, D. G. Cahill and E. Pop, *Nano Lett.*, 2010, **10**, 4363–4368.
10 K. F. Mak, C. H. Lui and T. F. Heinz, *Appl. Phys. Lett.*, 2010, **97**, 221904.
11 Y. Yue, J. Zhang and X. Wang, *Small*, 2011, **7**, 3324–3333.
12 K. I. Bolotin, K. J. Sikes, J. Hone, H. L. Stormer and P. Kim, *Phys. Rev. Lett.*, 2008, **101**, 096802–096804.
13 X. Du, I. Skachko, A. Barker and E. Y. Andrei, *Nat. Nanotechnol.*, 2008, **3**, 491–495.
14 Y. Q. Wu, P. D. Ye, M. A. Capano, Y. Xuan, Y. Sui, M. Qi, J. A. Cooper, T. Shen, D. Pandey, G. Prakash and R. Reifenberger, *Appl. Phys. Lett.*, 2008, **92**, 092102.
15 A. A. Balandin, S. Ghosh, W. Bao, I. Calizo, D. Teweldebrhan, F. Miao and C. N. Lau, *Nano Lett.*, 2008, **8**, 902–907.
16 A. A. Balandin, *Nat. Mater.*, 2011, **10**, 569–581.
17 S. Ghosh, I. Calizo, D. Teweldebrhan, E. P. Pokatilov, D. L. Nika, A. A. Balandin, W. Bao, F. Miao and C. N. Lau, *Appl. Phys. Lett.*, 2008, **92**, 151911.
18 R. R. Nair, P. Blake, A. N. Grigorenko, K. S. Novoselov, T. J. Booth, T. Stauber, N. M. R. Peres and A. K. Geim, *Science*, 2008, **320**, 1308.
19 D. Graf, F. Molitor, K. Ensslin, C. Stampfer, A. Jungen, C. Hierold and L. Wirtz, *Nano Lett.*, 2007, **7**, 238–242.
20 Z. H. Ni, H. M. Wang, J. Kasim, H. M. Fan, T. Yu, Y. H. Wu, Y. P. Feng and Z. X. Shen, *Nano Lett.*, 2007, **7**, 2758–2763.

21 L. Zhang, Z. Jia, L. M. Huang, S. O'Brien and Z. H. Yu, *J. Phys. Chem. C*, 2008, **112**, 13893–13900.
22 I. Calizo, A. A. Balandin, W. Bao, F. Miao and C. N. Lau, *Nano Lett.*, 2007, **7**, 2645–2649.
23 M. J. Allen, J. D. Fowler, V. C. Tung, Y. Yang, B. H. Weiller and R. B. Kaner, *Appl. Phys. Lett.*, 2008, **93**, 193119.
24 H. Harima, T. Hosoda and S. Nakashima, *J. Electron. Mater.*, 1999, **28**, 141–143.
25 D. Yoon, H. Moon, Y. W. Son, J. S. Choi, B. H. Park, Y. H. Cha, Y. D. Kim and H. Cheong, *Phys. Rev. B: Condens. Matter Mater. Phys.*, 2009, **80**, 125422.
26 N. Jung, A. C. Crowther, N. Kim, P. Kim and L. Brus, *ACS Nano*, 2010, **4**, 7005–7013.
27 J. W. Jiang, J. S. Wang and B. W. Li, *Phys. Rev. B: Condens. Matter Mater. Phys.*, 2009, **80**, 113405.
28 Z. Li and R. C. Bradt, *J. Appl. Phys.*, 1986, **60**, 612–614.

Published on 22 May 2014. Downloaded by Iowa State University on 27/06/2017 02:24:36.

 This journal is © The Royal Society of Chemistry 2014